Asian Journal of Chemistry; Vol. 38, No. 1 (2026), 187-194
ASIAN JOURNAL OF CHEMISTRY
https://doi.org/10.14233/ajchem.2026.34964

Unveiling the Oxidation Dynamics of Mefenamic Acid by Chloramine-T Using MnO/Ag_2O/NiO Nanoparticles

H.S. SONAKSHI, H.P. JAYADEVAPPA*, M.K. ARPITHA and K.M. VIDYASHREEN

Department of Chemistry, Yuvaraja's College, University of Mysore, Mysore-570006, India

*Corresponding author: E-mail: hpjayadevappa@gmail.com

Received: 26 September 2025 *Accepted*: 2 December 2025 *Published online*: 31 December 2025 AJC-22237

Green synthesis of sol-gel method was employed to synthesise MnO/Ag_2O/NiO nanoparticles. The synthesised nanoparticle showed an average crystalline size of 20-45 nm with semi-circular crystal structure. A combination of XRD, SEM, EDX and FTIR techniques provided insights into the material's size, shape and chemical composition. The data reveals the adverse catalytic property of the nanoparticle. The synthesised MnO/Ag_2O/NiO (MAN) nanoparticle was used as a catalyst to study the oxidation of mefenamic acid (MFA) by N-chloro-*p*-toluensulfonamide (CAT) in low pH solution at 298 K. A detailed analysis of the reaction stoichiometry and oxidation products was performed for both nano-catalyzed and non-nano-catalyzed reactions using LC-MS method. The influence of reaction rate on [CAT] is unimolecular, while the proportional to [MFA] is zero-order, for both nano-catalyzed and non-nano-catalyzed reactions. Influence of hydrogen ion concentration on reaction kinetics differs between the non-nanocatalyzed and nano-catalyzed reactions, with an inverse proportionality to a fractional power observed for the former and a non-integer order dependence observed for the latter. The reaction rate is not appreciably affected due to the accumulation of the resulting compound. A negligible negative correlation between the permittivity constant and reaction rate was found for both cases. The independence of the reaction rate on ionic strength implies that non-ionic species play a crucial role in the rate-limiting step. No evidence of free radical intermediates was found and kinetic studies at different temperatures enabled the calculation of thermodynamic parameters. A plausible mechanism was proposed to explain the observed kinetic parameters and rate laws were formulated for both catalyzed and nano-catalyzed reactions.

Keywords: Kinetics, Mefenamic acid, Chloramine-T, Nano-catalyzed, Mechanism, Stoichiometry.

INTRODUCTION

Mefenamic acid is an NSAID that helps reduce pain and inflammation by blocking prostaglandins, substances in the body that cause pain and swelling. By inhibiting the cyclo-oxygenase (COX) enzymes, mefenamic acid provides effect-tive relief from menstrual cramps, arthritis and musculo-skeletal disorders. When taken orally, mefenamic acid is absorbed by the body and then broken down by the liver before being excreted through kidneys [1-4]. However, it is essential to follow the recommended dosage and consult a healthcare professional before taking the medication, especially if you underlying medical conditions or are talking the other medi-cations. Mefenamic acid helps reduce pain and inflammation by blocking prostaglandins, but it is not suitable for everyone people with NSAID allergies, stomach ulcers or kidney prob-lems should use it with caution. By understanding the benefits and risks, individuals can make informed decisions about their treatment and work with their healthcare provider to find the best solution for their needs [5-8].

Chloramine-T is a powerful and versatile compound that plays a crucial role in various chemical reactions [9-11]. Its unique properties make it an effective oxidizing agent, capable of working efficiently in different environments, from acidic to basic conditions [12-14]. Chloramine-T is stable, mild and non-toxic, which makes it useful in many chemical applica-tions. It can carry out a wide range of molecular reactions, and its reaction behaviour is well studied and well understood [15]. Beyond its chemical significance, chloramine-T also boasts antimicrobial properties, making it a vital component in the fight against microbial diseases [16]. Its potential applications are vast and researchers continue to explore its capabilities in various fields. With its impressive profile, chloramine-T remains a significant entity in the world of organic chemistry [17-20].

Nanoparticles have transformed various industries due to their small size, high surface area and excellent absorption

properties, enabling smaller, faster and more efficient technologies. They can be synthesized through methods such as sol-gel, electrochemical, thermal and green synthesis. The electrochemical method, in particular, offers versatile and controllable nanoparticle production by reducing metal ions in solution, similar to green sol-gel approaches [21-25]. However, no studies have yet explored the degradation mefenamic acid using chloramine-T (CAT) and nanoparticles as catalysts. In this study, a comprehensive kinetic study of the catalyzed and uncatalyzed reactions of mefenamic acid by CAT in the presence of $MnO/Ag_2O/NiO$ (MAN) nanoparticles is investigated, exploring the underlying mechanistic and thermodynamic aspects in acidic aqueous medium at 298 K.

EXPERIMENTAL

Sol-gel synthesis: Approximately 6 g of dried *Hibiscus rosa-sinensis* leaves were boiled in 100 mL of double-distilled water for 3 h and then filtered. Separately, 1.5 g of $KMnO_4$, 0.5 g of MnO_2 and 1.5 g of $NiSO_4$ were dissolved and 2.5 g of $AgNO_3$ was dissolved in 50 mL of double-distilled water. These solutions were combined in a round-bottom flask and stirred at 900 rpm for 60 h using a magnetic stirrer. Hibiscus leaf extract was then added, along with 2 mL of acetic acid to maintain an acidic pH. The mixture was further heated and stirred for 4 h to optimize extraction. After cooling, the product was centrifuged, washed with deionized water and ethanol and dried in an oven at 700 ºC for 10 h through calcination, yielding the desired precipitate.

Experimental procedures: The experiment began with the preparation of a stable chloramine-T (CAT) solution in double-distilled water, standardized through iodometric titration and stored in a brown bottle to protect it from light. The $MnO/Ag_2O/NiO$ nanoparticles, synthesized through an eco-friendly sol-gel method, served as catalysts to facilitate the reaction. High-purity reagents and double-distilled water were used throughout to ensure consistent results. Potassium nitrate maintained ionic balance, while methanol was added in varying amounts to adjust the dielectric properties. By carefully controlling these conditions and employing advanced nanoparticle catalysts, the experiment aimed to optimize reaction efficiency and better understand the reaction dynamics.

Kinetic determination: To study the reaction kinetics, the experiment was designed under pseudo-unimolecular conditions with mefenamic acid in excess. Exact amounts of mefenamic acid, hydrochloric acid and sodium chloride were combined in a sealed tube to form the reaction mixture, which was maintained at 298 K. A measured amount of sodium tosylchloramide (CAT) solution was added and thoroughly mixed, with MAN nanoparticles serving as catalysts to accelerate the reaction. The unreacted CAT concentration was monitored over time using iodometric analysis to determine kinetic parameters. The results showed high reproducibility, with ±3% variation in the pseudo-unimolecular rate constant. Analysis of the kinetic data provided insights into the reaction mechanism and the kinetic order of each reactant, enabling a deeper understanding of the reaction dynamics.

Stoichiometry analysis as well as product identification of reaction: Thermodynamic equilibrium was achieved for a set of reaction solutions containing mefenamic acid, $MnO/Ag_2O/NiO$ nanoparticles and excess CAT after 48 h at 298 K. Excess CAT was used in the kinetic experiments and the amount of unreacted CAT present at the end of the reaction confirmed a 1:1 CAT-to- mefenamic acid stoichiometry. As a result, the stoichiometric equation was determined to be.

$$C_{15}H_{15}NO_2 + PTSO_2NClNa + H_2O \xrightarrow{MnO/Ag_2O/NiO} C_{15}H_{15}NO_3 + PTSO_2NH^+ + Na^+ + Cl^-$$

where $PT = CH_3C_6H_4$.

The predominant product of the reaction was determined as 2-[(2,3-dimethylphenyl)(oxidanyl)azan-1-yl]benzoic acid. Following evaluation, the most effective solvent for product extraction was found to 1,1'-oxybisethane. After treatment with aqueous NaOH, the ethereal layer was subjected to spot tests [26] using Dragendorff's and Ehrlich's reagents, which indicated the presence of an amine N-oxide moiety. *p*-Toluene sulfonide (PTS), the hydrogenation product of chloramine-T, was isolated in acetoxyethane and characterized by TLC using a mobile phase of ethoxyethane, trichloromethane and butyl hydroxide (2:2:1) with iodine as the detecting reagent, yielding a R_f value of 0.839.

RESULTS AND DISCUSSION

X-ray crystallography diffraction: XRD was utilized to analyse the crystallinity size 44 nm of the produced nano powder. In Fig. 1 shows that the two distinct peaks at 2θ = 37.20º and 43.20º can be correlated with the *hkl* values 111 and 200. These two peaks confirm the existence of NiO in the sample, which is well-matched with the standard JCPDS No. 04-0835. Three distinct diffraction peaks at 2θ = 27.94º, 32.27º and 54.92º can be correlated with the *hkl* value of 110, 111 and 220, respectively. These three peaks confirm the existence of Ag_2O in the sample, which is well-matched with the standard JCPDS No. 76-1393. Three distinct diffraction peaks at 2θ = 18.0º and 36.7º correspond to the (200) and (400) planes of α-MnO_2, while the peak at 2θ = 46.1º corresponds to the (210) plane of β-MnO_2.

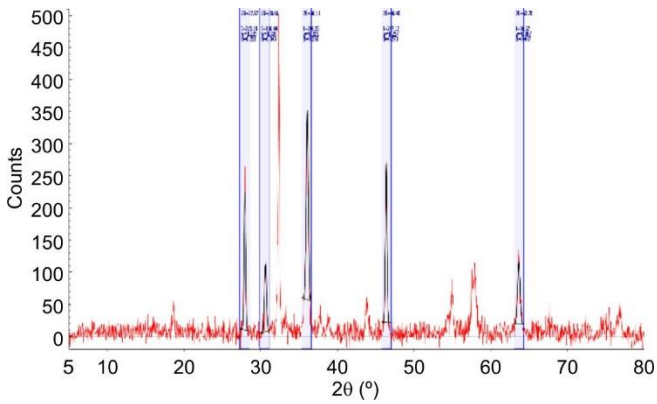

Fig. 1. XRD pattern of MAN nanoparticle

FE-SEM and EDS studies: The irregular or semi-circular crystals of nanoparticles shown length varies from 20-45 nm width varies from 1 to 5 μm. Over all shows medium to good morphology. Scanning electron microscopy (SEM) analysis

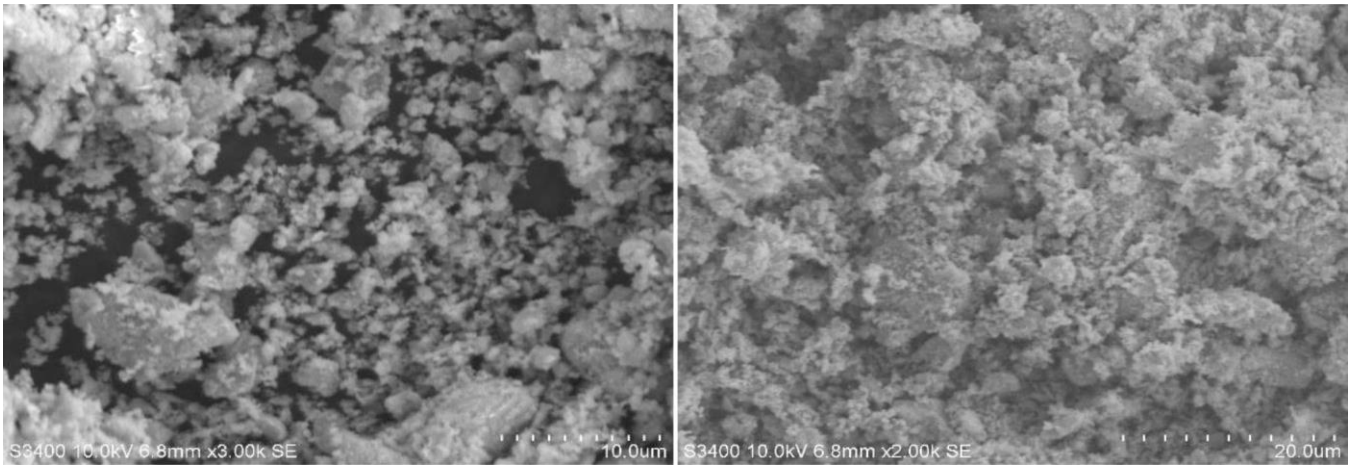

Fig. 2. SEM image of synthesized MAN nanoparticle

(Fig. 2) demonstrated that the catalytic activities of sol-gel synthesised nanoparticles are largely governed by their particle size and surface area. SEM analysis revealed that the sample consisted of agglomerated particles and EDAX were used to examine the elemental composition of the MAN nanoparticles. EDAX analysis confirms the elemental composition of the MnO/Ag_2O/NiO nanoparticle, as shown in the spectrum (Fig. 3). The graph shows distinct peaks corresponding to MnO/Ag_2O/NiO, indicating their presence in the prepared sample. The quantitative outcome from FE-SEM EDS examination, indicating the elemental composition, along with their relative proportions, are summarized in the accompanying data.

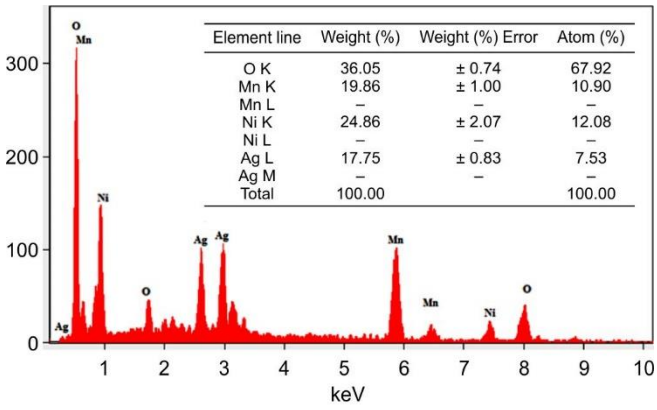

Fig. 3. X-ray analysis of EDS of the synthesized MAN nanoparticle

FTIR studies: To confirm the successful reduction and dispersion of chemical components, FTIR analysis facilitated the investigation of biological molecule-composite interactions in the fabrication of MnO, Ag_2O and NiO nanoparticles. The strong absorption signals at 614.68 and 629.51 cm^{-1} are attributed to the O-H stretching vibration in the amide group. Additional peaks at 1075.15, 2029.47 and 2209.99 cm^{-1} were observed, as shown in Fig. 4, representing the FTIR patterns of the MnO, Ag_2O and NiO nanoparticles.

Kinetic response of the reaction to reactant concentration changes: The kinetic study showed a pseudo-first-order reaction for the oxidation of mefenamic acid, with the rate dependent on the concentration of chloramine-T. The

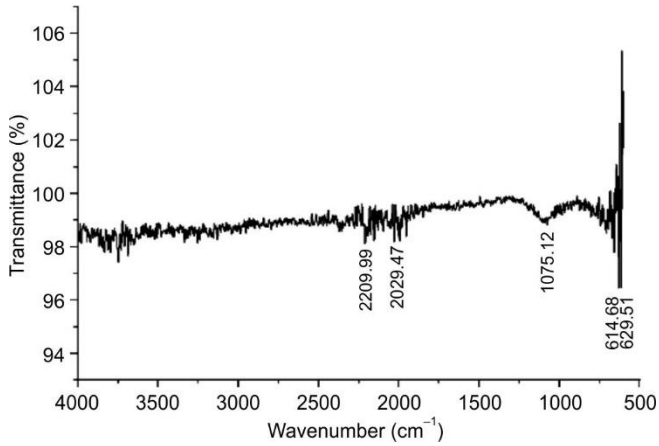

Fig. 4. FTIR patterns of MnO/Ag_2O/NiO nanoparticle

reaction was studied with and without MAN nanoparticles and the rate constant (k^I) was determined from the initial reaction rates. The results indicated a first-order dependence on the oxidant concentration. Under similar experimental conditions, the rate of reaction was independent of $[mefenamic\ acid]_0$ in both cases, suggesting a zero-order dependence of rate with respect to $[mefenamic\ acid]_0$ (Table-1).

Kinetic response of reaction to medium and catalyst: Fig. 5 shows that the rate of reaction increases with increase in $[H^+]$ and log-log plots of k^I and were linear (R^2 = 0.9863) with slope of 0.9 (positive), establishing the fractional-order dependence on $[H^+]$. A decreasing order in MnO/Ag_2O/NiO nanoparticle catalyst led to a decreasing in k^I and plots of log k^I *vs.* [MAN] nanoparticle catalyst was linear (R^2 = 0.9994) with a slope of -1.1225 (negative), demonstrates an inverse fractional order with respect to the nanocatalyst concentration.

Relationship between ionic strength and reaction kinetics: The influence of ionic strength on reaction kinetics was studied for both nanoparticle-catalyzed and non-catalyzed reactions by varying $[NaClO_4]$ from 0.1 to 1 mol L^{-1}, while maintaining constant experimental conditions. The negligible effect on reaction rate observed in both cases suggests that non-ionic species are involved in the rate-determining step, indicating a non-ionic mechanism governs the kinetics of both reaction pathways.

TABLE-1
INFLUENCE ON [MFA], [CHLORAMINE-T], [HYDROGEN ION], [CHLORIDE ION] THEN MAN ON THE OXIDATION OF THE MEFENAMIC ACID BY SODIUM TOSYLCHLORAMIDE, WITHOUT-NANO-CATALYST, WITH NANO-CATALYZED IN THE ACID SOLUTION AT 298 K

$10^3 \times$ [MFA] (mol L^{-1})	$10^5 \times$ [CAT] (mol L^{-1})	$10^3 \times$ [HCl] (mol L^{-1})	$10^4 \times$ [MAN] (g)	ku (s^{-1})	kc (s^{-1})
9	3	8	8	3.74	11.31
9	5	8	8	3.03	11.48
9	7	8	8	3.19	11.26
9	9	8	8	3.29	11.51
9	11	8	8	3.29	11.40
5	3	8	8	3.65	10.98
7	3	8	8	3.58	11.32
9	3	8	8	3.74	11.31
11	3	8	8	3.83	11.21
13	3	8	8	3.61	11.51
9	3	4	8	2.19	24.47
9	3	6	8	3.107	15.23
9	3	8	8	3.74	11.31
9	3	10	8	4.81	8.58
9	3	12	8	6.10	7.14
9	3	8	4	–	11.32
9	3	8	6	–	11.28
9	3	8	8	–	11.31
9	3	8	10	–	11.43
9	3	8	12	–	11.22

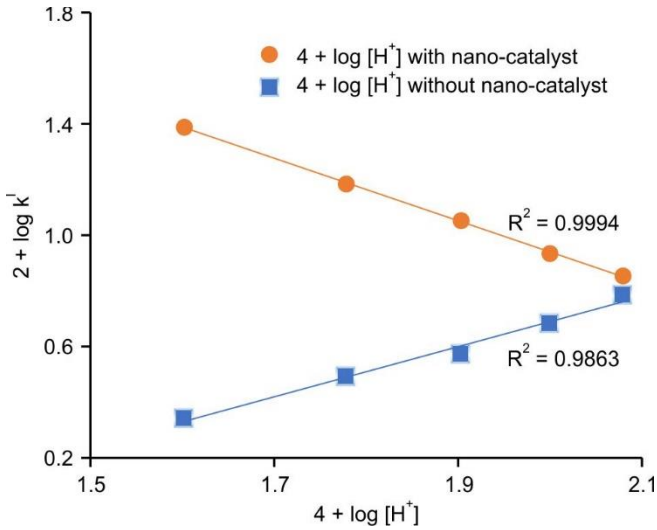

Fig. 5. Kinetic response on medium concentration at 298 K [Chloramine-T] = 3×10^{-4} mol L^{-1} [MAN] = 8×10^{-3} g

Electric permittivity of chemical reaction kinetics: The effect of dielectric permittivity on reaction kinetics was studied by varying the dielectric constant (D) of the reaction medium while keeping other parameters constant. Methanol was used as the solvent to examine its impact on both non-catalyzed and nanoparticle-catalyzed reactions. The results showed a consistent inverse relationship between reaction rate and dielectric permittivity across both reaction types (Table-2). The effect of dielectric permittivity on reaction kinetics was studied by adding methanol to the reaction medium in varying proportions (0-40% v/v). A linear correlation was observed between log k^I and the reciprocal of the dielectric

TABLE-2
KINECTS CHANGES WITH VARIATION OF DIELECTRIC PERMITTIVITY

CH_3OH (%v/v)	D	10^2/D	$ku^I 10^4$ (s^{-1})	$kc^I 10^4$ (s^{-1})
0	76.7	1.30	3.74	11.31
10	72.4	1.39	3.01	8.16
20	67.4	1.47	2.28	6.11
30	62.7	1.60	1.63	4.22
40	58.1	1.72	1.26	2.63

[CAT] = 3×10^{-4} mol/L, [MAN] = 8×10^{-3} g, [MFA] = 9×10^{-3} mol L^{-1}, [H^+] = 8×10^{-3} mol L^{-1}

constant (1/D), exhibiting a downward trend (Fig. 6). Control experiments confirmed that methanol ionization was negligible (< 1%) under the experimental conditions, ensuring it did not significantly impact the reaction kinetics.

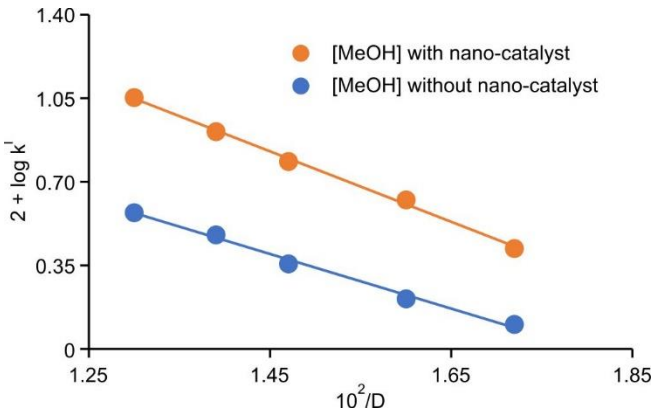

Fig. 6. Variation of dielectric permittivity on kinetics

Influence of product *para*-toluene sulfonamide concentration on the rate of reaction: The kinetics of the reaction were investigated using *para*-toluene sulfonamide (PTS) as an oxidant, with concentrations ranging from ($1 \times 10^{-4} - 10 \times 10^{-4}$ mol dm^{-3}). The results showed that PTS concentration had no significant impact on the reaction rate, indicating that it does not participate in the pre-equilibrium step for both non-catalyzed and nano-catalyzed reactions.

Thermal effects on chemical process dynamics: To investigate the effect of temperature on rates, a temperature range of 293-313 K was used to study the kinetics of both with nano-catalyzed and without nano-catalyzed reactions. A thorough analysis of the data presented in Table-3 indicates that the rate constant exhibits a consistent increase with thermal level for both with nano-catalyzed and without nano-catalyzed reactions. The linear Arrhenius plot depicted in Fig. 7 clearly indicates, temperature experts a profound influence on reaction kinetics, with the plot serving as a visual representation of this relationship. A thorough kinetic and thermodynamic analysis of the reaction was performed by assessing E_a variables with and without nanoparticle (Table-4).

Reaction mechanism without catalyst: The oxidation of mefenamic by CAT in the medium of water proceeded at the sluggish pace in the absence of nanocatalysts. The reaction involves each mole of mefenamic acid consumes one mole of CAT. The stoichiometric ration of mefenamic acid to CAT in the reaction is 1:1. A rate analysis of the chemical reaction

TABLE-3
VARIATION OF TEMPERATURE ON KINETICS OF CHEMICAL REACTION ON DEGRADATION OF MFA BY CAT IN ACID SOLUTION ALONG WITH ACTIVATION VARIABLES ON RATES

Temperature (K)	ku 10^4 (s^{-1})	kc 10^4 (s^{-1})
293	1.49	5.65
298	3.74	11.31
303	7.09	17.98
308	17.89	29.54
313	28.49	32.27

[CAT] = 3×10^{-4} mol dm^{-3}, [MnO/Ag_2O/NiO] = 8×10^{-3} g, [MFA] = 9×10^{-3} mol dm^{-3}, [H^+] = 8×10^{-3} mol dm^{-3}.

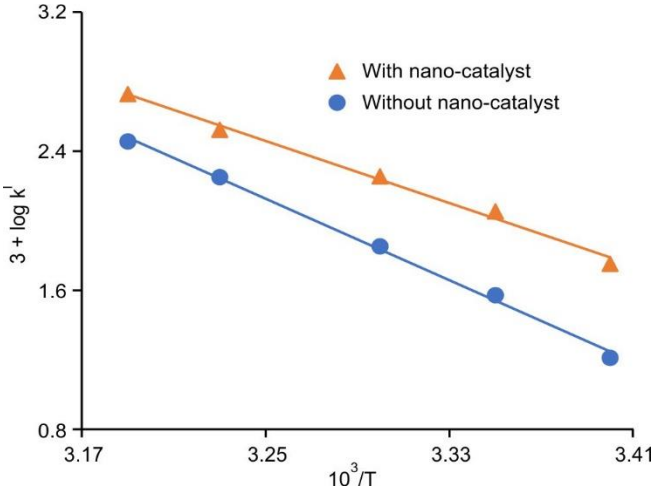

Fig. 7. Variation of temperature on kinetic of chemical reaction: A comparison of non-nano-catalyzed and nano-catalyzed systems

TABLE-4
THERMODYNAMICS PROFILE OF WITH NON-NANO CATALYZED AND NANO-CATALYZED REACTIONS

Activation variables	Non-nano-catalyzed	Nano-catalyzed
E_a (kJ mol^{-1})	112	68.06
$\Delta S^{\neq}$ (JK^{-1} mol^{-1})	63.0	-82.10
$\Delta H^{\neq}$ (kJ mol^{-1})	111.5	65.55
$\Delta G^{\neq}$ (kJ mol)	92.7	90.002

revealed a unimolecular order dependence on catalyst [CAT] whereas a non-integer order dependence on the concentration of [MFA] and hydrogen ions concentration.

Chloramine-T displays low oxidizing potential in acid and base mixtures, leading to reduction of substrates with a transfer of two electrons. In aqueous solution, it completely dissociates into ions, behaving as strong ionizer. In acidic water, it undergoes several equilibria, producing a range of ionic species [26-28].

$$PTSO_2NClNa \rightleftharpoons PTSO_2NCl^- + Na^+ \quad (2)$$

$$PTSO_2NCl^- + H^+ \rightleftharpoons PTSO_2NHCl \quad (3)$$

$$2\ PTSO_2NHCl \rightleftharpoons PTSO_2NH_2 + PTSO_2NCl_2 \quad (4a)$$

$$PTSO_2NCl_2 + H_2O \rightleftharpoons PTSO_2NHCl + HOCl \quad (5)$$

$$PTSO_2NHCl + H_2O \rightleftharpoons PTSO_2NH_2 + HOCl \quad (6)$$

where PT = $CH_3C_6H_4$ (*p*-toluene)

Scheme-I

Consequently, $PTSO_2NHCl$, $PTSO_2NCl_2$ and hypochlorous acid were recognized as the excellent oxidizer formed from chloramine-T in acidic aqueous solutions. Since the kinetics do not exhibit a second-order dependence on $[CAT]_0$, contrary to eqn. 4a, $PTSO_2NCl_2$ is excluded as a potential reactive species. Furthermore, the reaction kinetics are unaffected by the presence of N-chloro-4-methylbenzenesulfonamide, indicating that HCl does not play a primary role in the oxidation process. Therefore, $PTSO_2NHCl$ is identified as the reactive oxidant moiety. Under strongly acidic conditions (pH < 2), it protonates to form $PTSO_2NH_2Cl^+$ [29,30].

$$PTSO_2NHCl + H^+ \rightleftharpoons PTSO_2NH_2Cl^+ \quad (7)$$

The value of acid dissociation constant, according to eqn. 7, at standard temperature is found to be 1.02×10^2. The introduction hydrogen ions inhibit the reaction kinetics, suggesting that proton abstraction of $PTSO_2NH_2Cl^+$ produces the active oxidant moiety $PTSO_2NHCl$.

A mechanistic scheme was represented as rationalize experimental findings to the oxidation of mefenamic acid from chloramine-T. Here, $PTSO_2NHCl$ denotes the active oxidizing species, mefenamic acid represents the reactant entity, X and X^I signify the transition state complex the transition state complex entity formed during reaction course. The reaction is initiated by the formation of $PTSO_2NHCl$, which then reacts with the substrate to form an intermediate complex, X. This complex consequently undergoes a slowest elementary step in the reaction mechanism, yielding the X^I cation complex eliminating $PTSO_2NH_2$. Intermediate X^I undergoes hydrolysis to form Xa^{II}, followed by a reaction with $PTSO_2NHCl$ to generate the products, as shown in Schematic pathway-II.

$$PTSO_2NHCl + H^+ \overset{k_1}{\rightleftharpoons} PTSO_2NH_2Cl^+$$

(i) speedy reaction step

$$PTSO_2NH_2Cl^+ + MFA \overset{k_2}{\rightleftharpoons} X$$ (ii) speedy reaction step

$$X \overset{k_3}{\rightleftharpoons} X^I$$ (iii) rate determining step

$$X^I + H_2O \overset{k_4}{\rightleftharpoons} Products$$ (iv) speedy reaction step

The rate equation can be expressed differentially as follows:

$$\frac{d[CAT]}{dt} = k_3[X] \quad (8)$$

Let's assume $[CAT]_t$, which denote the overall active concentration of the chloramine-T, then:

$$[CAT]_t = [PTSO_2NH_2Cl^+] + [PTSO_2NHCl] + [X] \quad (9)$$

From equilibria (i) and (ii):

$$[B] \equiv [PTS_2NH_2Cl^+] = K_1[PTSO_2NHCl][H^+] \quad (10)$$

$$[X] = K_2[B][MFA] = K_1K_2[PTSO_2NHCl][H^+][MFA] \quad (11)$$

Eliminate $[PTSO_2NHCl]$ using eqns. 9-11. From (eqn. 9) we have:

$$[CAT]_t = [A]\ (1 + K_1[H^+] + K_1K_2[H^+][MFA])$$

with $[A] \equiv [PTSO_2NHCl]$,

So,

$$[A] = \frac{[CAT]t}{1 + K_1[H^+] + K_1K_2[H^+][MFA]}$$

Thus from (eqn. 11),

$$[X] = \frac{k_1 k_2 [H^+][MFA][CAT]t}{1 + K_1[H^+] + K_1 K_2 [H^+][MFA]}$$

Therefore, the rate becomes

$$r = -\frac{d[CAT]_t}{dt} = k_3[X] = k_3 \frac{k_1 k_2 [H^+][MFA][CAT]t}{1 + K_1[H^+] + K_1 K_2 [H^+][MFA]} \quad (12)$$

Eqn. 12 correctly predicts the experimental observed behaviour: pseudo-first order dependence (rate = k_1[CAT]t) with k_1 given by

$$k_1 = \frac{k_3 K_1 K_2 [H^+][MFA]}{1 + K_1[H^+] + K_1 K_2 [H^+][MFA]}$$

Rearrange (eqn. 12) to a reciprocal linear form useful for data analysis. Taking the reciprocal of k_1 yields:

$$\frac{1}{k_1} = \frac{1 + K_1[H^+] + K_1 K_2 [H^+][MFA]}{k_3 K_1 K_2 [H^+][MFA]} = \frac{1}{k_3 K_1 K_2 [H^+][MFA]} + \frac{1}{k_3 K_2 [MFA]} + \frac{1}{k_3} \quad (13)$$

From (eqn. 13) two linearization's are particularly useful:

(a) At constant [H^+] (vary [MFA]):

$$\frac{1}{k_1} = \left(\frac{1}{k_3 K_1 K_2 [H^+]} + \frac{1}{k_3 K_2} \right) \frac{1}{[MFA]} + \frac{1}{k_3}$$

A plot of $1/k_1$ *vs.* 1/[MFA] (at fixed [H^+]) is liner; slop and intercept give combinations of K_1, K_2, k_3

(b) At constant [MFA] (vary[H^+]):

$$\frac{1}{k_1} = \left(\frac{1}{k_3 K_1 K_2 [MFA]} \right) \frac{1}{[H^+]} + \left(\frac{1}{k_3 K_2 [MFA]} + \frac{1}{k_3} \right)$$

A plot of $1/k_1$ *vs.* 1/[H^+] (at fixed [MFA) is liner and yields additional relationships allowing independent determination of K_1, K_2, k_3

Thus the experimental approach of plotting $1/k_1$ *vs.* 1/[MFA] and $1/k_1$ *vs.* 1/[H^+] is justified and enables extraction of the equilibrium and rate constants. Notes on the observed fractional/inverse [H^+] dependence. Eqn. 12 does not automatically produce an inverse [H^+] dependence in every regime. An apparent inverse or fractional negative order in [H^+] can be obtained under realistic chemical circumstances if: (i) the effective concentration of reactive MFA depends on protonation equilibria (*i.e.*, neutral MFA is the reactive form and protonation sequesters it), or (ii) one or more equilibrium constants (*e.g.*, K_1 or K_2) themselves depend on [H^+] or ionic activities in a nontrivial (possibly fractional) way. Explicitly including the protonation equilibrium of MFA (or an H^+ dependence of K_1, K_2) produces inverse or fractional exponents in [H^+] consistent with experiment.

Dielectric and ionic strength effects, the negative slope in plots of ln k_1 *vs.* 1/D (D = dielectric constant) implies that dipole–dipole interactions contribute substantially to the transition-state stabilization. The insensitivity of the rate to ionic strength suggests a neutral transition state or non-ionic rate-limiting assembly. Slight inhibition by halide ions is consistent with weak competitive interactions at or near the reactive center. Thermodynamic parameters extracted from temperature dependence are consistent with a highly organized, low-entropy transition state (compact complex).

Reaction mechanism with MAN nanoparticle catalyst: A comparative kinetic study of the MAN nanoparticle-catalyzed and non-nanoparticle catalyzed oxidations of mefenamic acid (MFA) by chloramine-T (CAT) in acidic aqueous solution shows similar stoichiometry. Kinetic analysis indicates first-order dependence on [CAT] and a fractional (non-integer) dependence on acidity and nanoparticle concentration. The dielectric and thermodynamic results suggest a tightly bound, ordered transition state and a mechanism that involves a pre-equilibrium complex between CAT and the nanoparticle surface.

We denote:

- A = $PTSO_2NHCl$ (neutral oxidant),
- B = $PTSO_2NH_2Cl$ (protonated oxidant),
- NP = MAN nanoparticle (catalyst),
- X^{II} = Complex between B and NP (pre-equilibrium surface complex),
- X^{III} = subsequent adduct formed when MFA reacts with X^{II}.

Mechanistic steps (your labels preserved):

$$\text{(i)}\ A + B^+ \rightleftharpoons B \qquad (K_5, \text{fast}) \quad (14)$$

$$\text{(ii)}\ B + NP \rightleftharpoons X^{II} \qquad (K_6, \text{fast}) \quad (15)$$

$$\text{(iii)}\ X^{II} + MFA \xrightarrow{k_7} X^{III} + PTSO_2NH_2 \quad (\text{slow; RDS}) \quad (16)$$

$$\text{(iv)}\ X^{III} + H_2O \rightarrow \text{Products (fast)} \quad (16a)$$

Total experimentally active chloramine-T is

$$[CAT]_t = [A] + [B] + [X^{II}] \quad (17)$$

From equilibria (i) and (ii) we have

$$[B] = K_5[A][H^+], \quad [X^{II}] = K_2[B][NP] = K_5 K_6 [A][H^+][NP] \quad (18\text{-}20)$$

Hence

$[CAT]_t = [A] (1 + K_5[H^+] + K_5K_6[H^+][NP])$,

so

$$[A] = \frac{[CAT]_t}{1 + K_5[H^+] + K_5 K_6 [H^+][NP]} \quad (23)$$

Therefore

$$[X^{II}] = \frac{K_5 K_6 [H^+][NP][CAT]_t}{1 + K_5[H^+] + K_5 K_6 [H^+][NP]} \quad (24)$$

The rate (rate of disappearance of active CAT; choose positive r) is given by the slow step (iii):

$$r \equiv -\frac{d[CAT]_t}{dt} = k_7[X^{II}] = k_7 \frac{K_5 K_6 [H^+][NP][CAT]_t}{1 + K_5[H^+] + K_5 K_6 [H^+][NP]} \quad (25)$$

Define the pseudo-first-order constant k_c by $r = k_c[CAT]_t$. Then

$$k_c = \frac{k_7 K_5 K_6 [H^+][NP]}{1 + K_5[H^+] + K_5 K_6 [H^+][NP]} \quad (25a)$$

Eqn. 25a correctly predicts the experimentally observed behaviour:

Apparent first-order in [CAT](because $r \propto [CAT]_t$),

Fractional/non-integer dependence on [NP] and [H^+] through the equilibria and coverage terms,

Ionic-strength insensitivity when the reactive surface complex and transition state are overall neutral, and

No requirement for free-radical intermediates (inner-sphere surface pathway).

Linearisation's for parameter extraction:

Take the reciprocal of k_c:

$$\frac{1}{k_c} = \frac{1 + K_5[H^+] + K_5 K_6[H^+][NP]}{k_7 K_5 K_6[H^+][NP]} = \frac{1}{k_7 K_5 K_6[H^+][NP]} + \frac{1}{k_7 K_6[NP]} + \frac{1}{k_7} \quad (26)$$

Two useful experimental linearization's follow:

(A) At fixed [H^+] (vary [NP]): rearrange (eqn. 26) as a linear function of 1/[NP]:

$$\frac{1}{k_c} = \left(\frac{1}{k_7 K_5 K_6[H^+]} + \frac{1}{k_7 K_6}\right)\frac{1}{[NP]} + \frac{1}{k_7}$$

A plot of $1/k_c$ *vs.* 1/[NP] is linear; slope and intercept give combinations of K_5, K_6, k_7. Carrying out this fit at two or more [H^+] values allows separation of K_5 from K_6.

(B) At fixed [NP] (vary [H^+]): rearrange (eqn. 26) as a linear function of 1/[H^+]:

$$\frac{1}{k_c} = \left(\frac{1}{k_7 K_5 K_6[NP]}\right)\frac{1}{[H^+]} + \left(\frac{1}{k_7 K_6[NP]} + \frac{1}{k_7}\right)$$

A plot of $1/k_c$ *vs.* 1/[H^+] at fixed [NP] is linear and yields additional independent constraints.

From the family of slope/intercept values obtained at differing [H^+] and [NP], you can extract numerical values for K_5, K_6 and k_7 by standard linear regression and simultaneous solution of the parameter combinations.

Conclusion

The cross-comparison analysis comparative study of oxidation of mefenamic acid by Chloramine-T (CAT) in of both with MnO/Ag_2O/NiO (MAN) nanoparticle catalyzed and without nanoparticle-catalyzed reactions are investigated. The catalytic potency of MAN nanoparticle for oxidation of mefenamic acid by CAT in a water-based acidic environment was studied by comparing with the uncatalyzed reactions. The CAT-MFA redox reaction has examined in aqueous-based acidic environment. The oxidation of mefenamic acid by CAT exhibits a 1:1 stoichiometry, regardless of whether nanoparticles are present to catalyze the reaction and LC-MS analysis is done for reactant and product. The oxidation products were identified as 2-[(2,3-dimethylphenyl)(oxidanyl)-azan-1-yl]-benzoic acid. The effects of halide ions and dielectric permittivity on the reaction kinetics were investigated. Activation parameters, including activation energy, entropy, free energy and enthalpy, were determined using Arrhenius analysis of the experimentally observed rate constants, providing insight into the reaction mechanism and allowing the derivation of the rate law. The results indicate that MAN nanoparticles, prepared *via* sol-gel synthesis, exhibit the catalytic activity that enhances the oxidation of mefenamic acid by chloramine-T, demonstrating their potential for applications in environmental remediation.

ACKNOWLEDGEMENTS

The authors gratefully acknowledge the support of Mysore University, Mysuru, for providing access to instrumental and laboratory resources in the Chemistry Department, Yuvaraja's College, which facilitated the kinetic studies.

CONFLICT OF INTEREST

The authors declare that there is no conflict of interests regarding the publication of this article.

DECLARATION OF AI-ASSISTED TECHNOLOGIES

During the preparation of this manuscript, the authors used an AI-assisted tool(s) to improve the language. The authors reviewed and edited the content and take full responsibility for the published work.

REFERENCES

1. N. Cimolai, *Expert Rev. Clin. Pharmacol*., **6**, 289 (2013); https://doi.org/10.1586/ecp.13.15
2. M. Moore and P. Little, *Cochrane Libr.*, **2011**, CD007553 (2011); https://doi.org/10.1002/14651858.CD002870.pub3.
3. U. Pai, R.A. Venkata, A. Shah, A. Gupta, A. Clement, A. Wadhwa, A. Kumar, A. Somasundaram, G. Charde, K.K. Joshi, M. Sanklecha, M. V.S. Kumar, P. Gokhale, R. Agarwal, R. Shah, R. Chhabra, S. Niranjan, S. Dudhgaonkar, S. Surampudi, S. Nayak and V.V. Borkar, *Cureus*, **17**, e88412, (2025): https://doi.org/10.7759/cureus.88412
4. J. Guzmán-Esquivel, H. Galvan-Salazar, H. Guzman-Solorzano, A. Cuevas-Velazquez, J. Guzman-Solorzano, K. Mokay-Ramirez, B. Paz-Michel, E. Murillo-Zamora, J. Delgado-Enciso, V. Melnikov, O. Delgado-Enciso, I. Rodriguez-Sanchez, M. Martinez-Fierro, F. Rojas-Larios, M. Walle-Guillen, C. Cardenas-Aguilar, O. Beas-Guzman, D. Chaviano-Conesa, H. Garcia-Garcia and I. Delgado-Enciso, *Int. J. Mol. Med.*, **49**, 29 (2022); https://doi.org/10.3892/ijmm.2022.5084
5. P.S. Khansari and R.F. Halliwell, *Front. Neurosci.*, **13**, 64 (2019); https://doi.org/10.3389/fnins.2019.00064
6. M. Vahedi, S.B. Hasanpoor-Azghady, L. Amiri-Farahani and I. Khaki, *Trials*, **22**, 655 (2021); https://doi.org/10.1186/s13063-021-05622-w
7. F. Shabani, F. Narenji, K. Vakilian, M.A. Zareian, M. Bozorgi, S. Bioos and F. Nejatbakhsh, *Open Public Health J.*, **15**, 34 (2022); https://doi.org/10.2174/18749445-v15-e2205190
8. J.K. Gupta and J. Kai, *Int. J. Basic Clin. Pharmacol.*, **7**, 1132 (2018); https://doi.org/10.18203/2319-2003.ijbcp20182638
9. S. Shidhaye, V.J. Kadam and S. Malke, *Indian J. Pharm. Sci.*, **69**, 211 (2007); https://doi.org/10.4103/0250-474X.33145
10. E. Kolvari, A. Ghorbani-Choghamarani, P. Salehi, F. Shirini and M.A. Zolfigol, *J. Iran. Chem. Soc.*, **4**, 126 (2007); https://doi.org/10.1007/BF03245963
11. A. Sukhdev, A.S. Manjunatha and P. Puttaswamy, *ISRN Phys. Chem.*, **2013**, 738932 (2013); https://doi.org/10.1155/2013/738932
12. Puttaswamy and R.V. Jagadeesh, *Ind. Eng. Chem. Res.*, **45**, 1563 (2006); https://doi.org/10.1021/ie0509746
13. Y.N. Nayak, S.L. Gaonkar, E.A.M. Saleh, A.M.A.L. Dawsari, Harshitha, K. Husain and I. Hassan, *J. Saudi Chem. Soc.*, **26**, 101416 (2022); https://doi.org/10.1016/j.jscs.2021.101416
14. T. Umemoto, S. Fukami, G. Tomizawa, K. Harasawa, K. Kawada and K. Tomita, *J. Am. Chem. Soc.*, **112**, 8563 (1990); https://doi.org/10.1021/ja00179a047
15. G. Agnihotri, *Synlett*, **18**, 2857 (2005); https://doi.org/10.1055/s-2005-918936

16. K. Mangal, M.M. Dhamande, S. Sathe, R. Patel and C. Dahihandekar, *Cureus*, **14**, e33200 (2022); https://doi.org/10.7759/cureus.33200
17. K.M. Meenakshi and K.V. Pai, *J. Chem.*, **6**, 545 (2009); https://doi.org/10.1155/2009/149032
18. P.T. Sowmya, K.M.L. Rai, A. Sudhir and S.Y. Kotian, *Aust. J. Chem.*, **74**, 689 (2021); https://doi.org/10.1071/CH21089
19. J. Ungula and H.C. Swart, *J. Alloys Compd.*, **821**, 153459 (2020); https://doi.org/10.1016/j.jallcom.2019.153459
20. A.F. Abdel Hakiem, A.M. Kamal, A.S. Aboraia, R.M. Mahfouz, A.A.K. Mohammed, I.A. Naguib and M.E. Draz, *Microchem. J.*, **206**, 111423 (2024); https://doi.org/10.1016/j.microc.2024.111423
21. D.-Q. He, Y.-J. Zhang, D.-N. Pei, G.-X. Huang, C. Liu, J. Li and H.-Q. Yu, *J. Hazard. Mater.*, **383**, 121090 (2020); https://doi.org/10.1016/j.jhazmat.2019.121090
22. Z.Y. Shnain, M.F. Abid and K.A. Sukkar, *Desalin. Water Treatment*, **210**, 22 (2021); https://doi.org/10.5004/dwt.2021.26581
23. M. Rathod, P.G. Moradeeya, S. Haldar and S. Basha, *Photochem. Photobiol. Sci.*, **17**, 1301 (2018); https://doi.org/10.1039/c8pp00156a
24. M. Ebrahimi and O. Akhavan, *Catalysts*, **12**, 667 (2022); https://doi.org/10.3390/catal12060667
25. F. Feigl and V. Anger, Spot Test in Organic Analysis, Elsevier, Amsterdam, edn 7, p. 376 (2005)
26. J.C. Morris, J.A. Salazar and M.A. Wineman, *J. Am. Chem. Soc.*, **70**, 2036 (1948); https://doi.org/10.1021/ja01186a016
27. E. Bishop and V.J. Jennings, *Talanta*, **1**, 197 (1958); https://doi.org/10.1016/0039-9140(58)80034-X
28. F.F. Hardy and J.P. Johnston, *J. Chem. Soc., Perkin Trans. II*, 742 (1973); https://doi.org/10.1039/p29730000742
29. B.G. Pryde and F.G. Soper, *J. Chem. Soc.*, 1514 (1931); https://doi.org/10.1039/JR9310001514
30. A. Sukhdev and P. Puttaswamy, *Springerplus*, **2**, 30 (2013); https://doi.org/10.1186/2193-1801-2-30
31. D.K. Wolgemuth, S.D. Elmore, J.D. Cope, P.E. Sheridan, S.L. Stokes and J.P. Emerson, *Catal. Commun.*, **150**, 106275 (2021); https://doi.org/10.1016/j.catcom.2020.106275
32. E.S. Amis, Solvent Effects on Reaction Rates and Mechanism, Academic Press: New York, p. 1672 (1966; reprint 2007).
33. K.J. Laidler, Chemical Kinetics, Tata McGraw-Hill, New Delhi, edn 3, p. 544 (2003).